INTERNATIONAL JOURNAL FOR NUMERICAL METHODS IN FLUIDS
Int. J. Numer. Meth. Fluids 2001; **37**: 951–986 (DOI: 10.1002/fld.199)

Footbridge between finite volumes and finite elements with applications to CFD

Frédéric Pascal[a,b,*,1] and Jean-Michel Ghidaglia[a,2]

[a] *Centre de Mathématiques et de Leurs Applications, ENS Cachan et CNRS UMR 8536, F-94235 Cachan Cedex, France*
[b] *Laboratoire de Mathématique, UMR 8628, CNRS et Université Paris-Sud, Bâtiment 425, Université Paris-Sud, F-91405 Orsay Cedex, France*

SUMMARY

The aim of this paper is to introduce a new algorithm for the discretization of second-order elliptic operators in the context of finite volume schemes on unstructured meshes. We are strongly motivated by partial differential equations (PDEs) arising in computational fluid dynamics (CFD), like the compressible Navier–Stokes equations. Our technique consists of matching up a finite volume discretization based on a given mesh with a finite element representation on the *same* mesh. An inverse operator is also built, which has the desirable property that in the absence of diffusion, one recovers *exactly* the finite volume solution. Numerical results are also provided. Copyright © 2001 John Wiley & Sons, Ltd.

KEY WORDS: compressible fluids and gas dynamics; finite element methods; finite numerical method; finite volume methods

1. INTRODUCTION

Finite volume schemes are widely used in numerical solutions to conservation laws, such as those occurring in computational fluid dynamics (CFD) and especially in complex multidimensional fluid flow problems. The basic idea for constructing finite volume methods consists in integrating over a finite control volume the divergence form of the differential equation and in using Green's formula to convert the result into surface integrals of fluxes that are then discretized.

The interest of these methods stems from (i) their compactness in terms of numerical stencil, (ii) their natural goodness of fit for the approximation of conservation laws, and (iii) their effectiveness on unstructured multidimensional meshes. When considering flows with

* Correspondence to: Centre de Mathématiques et de Leurs Applications, ENS Cachan et CNRS UMR 8536, 61 ave. du Président Wilson, F-94235 Cachan Cedex, France.
[1] E-mail: frederic.pascal@cmla.ens-cachan.fr
[2] E-mail: jmg@cmla.ens-cachan.fr

Received 30 September 1999
Revised 11 January 2001

discontinuities (shock capturing, low dissipation, ...) or non-linear hyperbolic-dominated flows, finite volume methods have shown their efficiency by conforming within the upwind strategy and by ensuring robust, stable and convergent schemes.

Nevertheless, it may be necessary to compute some discrete gradients of the solution, e.g. (i) for the implementation of higher-order schemes or (ii) for the discretization of second-order elliptic operators.

Let us discuss the implementation of higher-order schemes. In the extension of Godunov's scheme to second-order accuracy in one space dimension (MUSCL scheme), Van Leer [1] based the numerical advection on the reconstruction of a piecewise linear function. Generalizations to multidimensional flows and to unstructured meshes of this scheme have been proposed by Barth [2] and Abgrall [3,4]; they needed reconstruction algorithms up to any order of accuracy, limiting procedures and essentially non-oscillatory techniques. For other multidimensional schemes, the reader is referred to Godlewski-Raviart [5] and references therein.

Concerning the discretization of viscous fluxes arising in diffusion–convection-like problems, a computational solution lying on the four points scheme has been widely studied by Eymard *et al.* [6], Vignal [7] and Herbin [8] from a numerical and a theoretical point of view. But some geometrical assumptions have to be satisfied: every angle θ of a triangle belonging to the mesh must satisfy $\eta < \theta < \pi/2 - \eta$ (with $\eta > 0$), and in some case, the size of all triangles must be of the same order.

On the opposite side, centered finite element approximations, which are well suited for second-order operators, suffer from too strong diffusion or may involve some numerical instability in case of a too large Peclet number, i.e. a small physical viscosity. A classical technique, in order to cure these drawbacks, is the streamline upwind Petrov–Galerkin method (see Brooks and Hughes [9]), which is inspired from the upwind strategy well suited to purely convective problems.

Then, an attractive alternative for the computation of gradients consists in combining finite element and finite volume methods. Let us first mention the finite volume element method (see Liu and McCormick [10] and Cai *et al.* [11,42]), where the solution of elliptic problems is sought in a finite dimension space of piecewise smooth functions by using a finite set of control volumes defined by the circumcenter of the triangles. These schemes have been viewed as a finite element method (with the unknowns located at the vertices of meshes) and their error estimates have followed from the finite element theory.

There also exists a mixed finite volume–finite element formulation (sometimes called weighted finite volume scheme), which has been introduced for Euler equations by Dervieux [12] and discussed by Selmin [13]. This scheme extended to compressible Navier–Stokes equations by Rostand and Stoufflet [14] is widely used in works of Eymard *et al.* [6], Arminjon and Madrane [15], Carré and Dervieux [16], Debiez *et al.* [17], Dervieux and Desideri [18], Farhat and Lanteri [19], Guillard [20], Guillard and Viozat [21], Lanteri [22], Le Ribault *et al.* [23], Mer [24], etc. The method is based on the combination of a Galerkin finite element method for the diffusive part of the system and of a vertex finite volume scheme for the discretization of the convective part: indeed, the latter allows us to introduce flux splitting and upwinding techniques. The approximate solution is located at the vertices of the mesh, control volumes are formed from faces of the dual mesh connecting the centroids of triangles through medians and the finite element is the classical conforming linear finite element. Moreover, if a

linear approximation is used and if mass is lumped or if low-order quadrature formulas are employed, it can be shown that this scheme is equivalent to the conforming finite element method (see, for instance, Idelsohn and Onate [25] and references therein). Feistauer *et al.* [26] have mathematically derived the same approach and have established some theoretical results for the scalar non-linear convection–diffusion problem (see Feistauer *et al.* [27] for the convergence analysis of the explicit scheme, Feistauer *et al.* [28] for the convergence analysis of the implicit version, Feistauer *et al.* [29] for an estimate of the error). This large class of schemes tries to take profit from the advantages of both finite element and finite volume methods, but these schemes may involve much more numerical viscosity than necessary and the vertex finite volume method presents some drawbacks. Some high-order difference for artificial dissipation terms and some high-order upwinding have to be combined with these formulations and implies the computation of gradients.

More recently, Dolejsi and Angot [30] and Feistauer *et al.* [31] developed for the discretization of non-linear convective–diffusion equations, a method by combining a barycentric finite volume and a non-conforming triangular piecewise-linear finite element scheme. Their control volumes are defined by joining the barycenter of each triangle with its vertices and the solution is located at the middle of the interfaces. Convergence and some *a priori* error estimates are established in Angot *et al.* [32] and Dolejsi *et al.* [Dolejsi V, Feistauer M, Felcman J, Klikova A. Error estimates for barycentric finite volumes combined with non-conforming finite elements applied to non-linear convection–diffusion problems. To appear in *Applications of Mathematics*].

Let us remark that in the context of the cell finite volume scheme (where control volumes are the triangles of the mesh), it would be possible to use an adjoint mesh, where vertices are the centroids of triangles of the primal mesh (Dolejsi, private communication) in order to associate with the finite volume approximation a conforming finite element formulation. But beside the fact that some vertices on the boundaries have to be added, it requires the complete building of a secondary mesh.

For time-dependent compressible viscous flow problems, our aim is to propose a new numerical way to discretize diffusion operators in the context of cell finite volume scheme. We are motivated in developing a method to treat numerically second-order operators without any constraint on the mesh, without building a dual mesh and without introducing any numerical diffusion. Since finite element schemes are naturally well fitted for the discretization of second-order operators like the diffusion operator, we propose a numerical algorithm based on footbridges between the finite volume representation of functions and a finite element one where footbridges are operators between the discretized spaces. Let us emphasize that both spaces are defined on the same given mesh without building an auxiliary mesh.

In Section 2, we introduce the principle of footbridges for two-dimensional domains and we discuss the essential features of a strategy using it to solve a scalar convection–diffusion problem: we particularly emphasize the computational aspect of the scheme. Section 3 introduces a more relevant footbridge, which is more suited to problems with small physical diffusion and which we use in the numerical experiments. In Section 4, we build a footbridge that preserves 'the mass', i.e. $\int_\Omega u \, \mathrm{d}x$. The method is tested on the two-dimensional scalar and linear convection–diffusion problem in Section 5. Some numerical results of convergence by comparing the solution with an overkilled solution are provided. Then the algorithm is

incorporated into a gas dynamics finite volume code. For a demonstration of the good behavior of the method, we consider first a two-dimensional extention of the shock-tube problem and second the flow past a NACA0012 airfoil, where meshes are used with different element sizes and aspect ratios without any constraint (except the basic finite element ones).

2. MOTIVATIONS AND PRINCIPLE OF THE FOOTBRIDGES

For time-dependent viscous problems, we think that an efficient method has to be based on a good solver of the inviscid part: the natural goodness of fit of finite volume methods leads us to keep these methods. In the context of cell finite volume scheme (where control volumes are the triangles of the mesh), the discretization of the second-order operator is a particularly difficult task. But the natural goodness of fit for the viscous part of finite element methods induces us to match up the finite volume representation of the solution with a finite element function. And this latter representation allows to easily discretize the viscous operator thanks to a variational formulation.

We first define two discretized function spaces: the space of finite volumes and the space of finite elements, both defined on the *same given mesh* without building an auxiliary mesh. The first part of this section is concerned with the definition of these two spaces and with the definitions of footbridges. The finite element solution is simply defined by the natural L^2 projection of the piecewise constant finite volume function. The inverse operator consists also in the L^2 projection this time on the finite volume space. At the end of the section, this idea will appear to be a naïve one.

Let us note that the type of the finite element (here Crouzeix and Raviart [33] finite element) is chosen *a posteriori* in order to be able to build an inverse footbridge. Indeed, after the viscous step, the finite element representation of the solution has to be reverted to a finite volume form (i.e. cell piecewise constant function) in order to be convected. The building of the inverse footbridge is done in such a way that it presents no error in the case of zero physical diffusion.

The treatment of the viscous and the convective operators is realized with a time-splitting strategy, which on one hand allows us to use highly specialized methods to solve each steps and on the other hand, from a practical point of view at least, allows us to modify an existing code for solving hyperbolic systems with cell finite volumes by adding the two footbridge steps and a finite element discrete viscous operator.

The second part of this section describes the fractional steps: (i) an inviscid step in the finite volume space, (ii) the projection of the solution on the finite element space (direct footbridge), (iii) a viscous step in the finite element space, (iv) the transform of the finite element representation in a finite volume one (inverse footbridge).

2.1. Notations

We denote by Ω the computational domain, a bounded open set of $\mathbb{R}^2$ with a polygonal boundary. Let $\mathscr{T}$ be a triangular mesh of Ω: $\Omega = \cup_{T\in\mathscr{T}} T$.

Let χ_α be the piecewise-constant characteristic function defined on each triangle T_α

$$\chi_\alpha(x) = 1 \quad \text{if } x \in T_\alpha \quad \text{and} \quad 0 \text{ elsewhere}$$

For each edge A_j of the mesh, let us define the piecewise linear function φ_j such that

- $\varphi_j(M) = 1$ if M is the center of A_j
- $\varphi_j(M) = 0$ if M is the center of an edge different from A_j

We denote by $\mathscr{V}$ the finite volume space, spanned by the χ_α, where T_α belongs to $\mathscr{T}$ and by $\mathscr{E}$ the non-conforming piecewise linear finite element space, spanned by the φ_j functions. The set $\mathscr{E}$ is the space consisting of $P1$ discontinuous functions defined by Crouzeix and Raviart [33]. Concerning error estimates, this finite element has the same bahavior as the classical Lagrange linear finite element.

The dimension of $\mathscr{V}$ is equal to the number of triangles, NE, and the dimension of $\mathscr{E}$ is equal to the number of edges, NF. Let us recall that if NS is the number of vertices, one gets the Euler formula

$$NS + NE = NF + g + 1$$

where g is the genus of Ω. Hence, asymptotically when $NE \to \infty$, one has

$$NS \sim \frac{NE}{2} \quad \text{and} \quad NF \sim \frac{3}{2} NE$$

It is then straightforward that there is no one to one linear function between $\mathscr{V}$ and $\mathscr{E}$.

Nevertheless, to each v in $\mathscr{V}$, we associate an element in $\mathscr{E}$ denoted $u = \Pi_{EV} v$, which is obtained as the solution of the following least square problem: u in $\mathscr{E}$ solution of

$$\int_\Omega |u(x) - v(x)|^2 \, \mathrm{d}x = \min_{w \in \mathscr{E}} \int_\Omega |w(x) - v(x)|^2 \, \mathrm{d}x \tag{1}$$

so that

$$\int_\Omega (u - v)\varphi_j \, \mathrm{d}x = 0 \quad \forall j = 1, \ldots, NF \tag{2}$$

Similarly, to each u in $\mathscr{E}$, we first construct $v = \Pi_{VE} u$ in $\mathscr{V}$ solution of

$$\int_\Omega |v(x) - u(x)|^2 \, \mathrm{d}x = \min_{w \in \mathscr{V}} \int_\Omega |w(x) - u(x)|^2 \, \mathrm{d}x \tag{3}$$

which yields

$$\int_\Omega (u - v)\chi_\alpha \, \mathrm{d}x = 0 \quad \forall \alpha = 1, \ldots, NE \tag{4}$$

Since it is convenient to use co-ordinate formulation, let us rewrite (2) and (4). We notice that the mass matrix in (2) is diagonal in space dimension two and the ith coefficient is given by

- $\dfrac{|T_\alpha| + |T_\beta|}{3}$ if i is the edge $T_\alpha \cap T_\beta$
- $\dfrac{|T_\alpha|}{3}$ if the edge i is on the boundary $\partial\Omega$

Then for $v = \Sigma_{\alpha=1}^{NE} a_\alpha \chi_\alpha$ one gets $\Pi_{EV} v = \Sigma_{j=1}^{NF} u_j \varphi_j$ with

- $u_j = \dfrac{|T_\alpha| v_\alpha + |T_\beta| v_\beta}{|T_\alpha| + |T_\beta|}$ if j is the number of the common edge of triangles T_α and T_β
- $u_j = v_\alpha$ if j is the number of an edge belonging to $\partial\Omega$

For $u = \Sigma_{j=1}^{NF} u_j \varphi_j$, system (4) yields $\Pi_{VE} u = \Sigma_{\alpha=1}^{NE} v_\alpha \chi_\alpha$ with

$$v_\alpha = \frac{u_j + u_k + u_l}{3}$$

where j, k, l are the T_α edge numbers.

2.2. Application of the footbridges to a scalar equation

To fix ideas and without losing any generality, we shall consider here the two-dimensional scalar convection–diffusion equation

$$\frac{\partial \omega}{\partial t} + \operatorname{div}(\omega C) = \nu \Delta \omega \quad \text{in } \Omega \tag{5}$$

where C is a constant vector of $\mathbb{R}^2$ and $\nu > 0$ is the diffusion parameter. The function $\omega = \omega(x_1, x_2, t)$ is a real function.

We use a time-splitting strategy for separating each operator and we refer to the footbridge previously defined for solving Equation (5) numerically. Let us suppose that at each instant t^n, we get two approximations ω^n of the function $\omega(\,.\,, t^n)$, one belonging to the finite volume space $\mathscr{V}$ and the other one to the finite element space $\mathscr{E}$. We proceed by showing how to compute the next time step approximation of the solution.

Considering the initial value problem

$$\frac{\partial \omega}{\partial t} + \operatorname{div}(\omega C) = 0 \tag{6}$$

where the initial data are the finite volume representation $\omega^n \in \mathscr{V}$, one can compute easily an optimal upwind numerical discrete flux written under the form

$$\sum_{T_\beta \in \mathscr{N}(T_\alpha)} \phi^n_{C_{\alpha,\beta}}$$

for all T_α of the triangulation $\mathscr{T}$. We denote $\mathscr{N}(T_\alpha)$ as the set of the neighboring triangles of T_α. Hence the approximation of the solution to (6) after a time step Δt_n is given by

$$\omega_\alpha^{n+1} = \omega_\alpha^n - \Delta t_n \sum_{T_\beta \in \mathscr{N}(T_\alpha)} \phi^n_{C_{\alpha,\beta}}, \quad \forall T_\alpha \in \mathscr{T}$$

In case of a linear problem, all the upwind schemes yield the following flux:

- $\phi^n_{C_{\alpha,\beta}} = |T_\alpha \cap T_\beta| \omega_\alpha^n C \cdot \vec{v}_{\alpha\beta}$ if $C \cdot \vec{v}_{\alpha\beta} > 0$
- $\phi^n_{C_{\alpha,\beta}} = |T_\alpha \cap T_\beta| \omega_\beta^n C \cdot \vec{v}_{\alpha\beta}$ if $C \cdot \vec{v}_{\alpha\beta} < 0$
- $\phi^n_{C_{\alpha,\beta}} = 0$ if $C \cdot \vec{v}_{\alpha\beta} = 0$

where $\vec{v}_{\alpha\beta}$ denotes the normal vector from the triangle T_α toward the triangle T_β. An implicit scheme could be implemented, but we do not want to address this question here and we refer to Ghidaglia *et al.* [34].

At the same time, we solve the following diffusion equation, where the initial data are the finite element representation $\omega^n \in \mathscr{E}$:

$$\frac{\partial \omega}{\partial t} = \nu \Delta \omega \tag{7}$$

with the non-conforming finite element method (related to $\mathscr{E}$) and a forward Euler time scheme. Hence $\omega^{n+1} \in \mathscr{E}$ is solution to the linear system

$$\int_\Omega \left(\frac{\omega^{n+1} - \omega^n}{\Delta t_n} \right) \varphi_j \, \mathrm{d}x = -\nu \sum_{\alpha=1}^{NE} \int_{T_\alpha} \Delta \varphi_j \cdot \nabla \omega^{n+1} \, \mathrm{d}x, \quad \forall j = 1, \ldots, NF \tag{8}$$

This latter integral makes sense since ω^{n+1} and φ_j are linear on each T_α. Now since the φ_j are continuous along the normal direction to the edges, we get

$$\sum_{\alpha=1}^{NE} \int_{T_\alpha} \nabla \varphi_j \cdot \nabla \omega^{n+1} \, \mathrm{d}x = \int_\Omega \nabla \varphi_j \cdot \nabla \omega^{n+1} \, \mathrm{d}x \tag{9}$$

Finally, our approach yields the following algorithm:

- **1.** Construct an approximate solution $\omega^0 \in \mathscr{V}$ of the initial data ω_0 with, for instance

$$\omega_\alpha^0 = \frac{1}{|T_\alpha|} \int_{T_\alpha} \omega_0(x) \, \mathrm{d}x, \quad \forall \alpha = 1, \ldots, NE$$

- **2.** Compute $\omega^{n,1} \in \mathscr{V}$ solution at time $t^n + \Delta t_n$ of Equation (6) with the initial value $\omega^n \in \mathscr{V}$ by using

$$\omega_\alpha^{n,1} = \omega_\alpha^n - \Delta t_n \sum_{T_\beta \in \mathcal{N}(T_\alpha)} \phi^n_{C_{\alpha,\beta}}, \quad \forall \alpha = 1, \ldots, NE$$

- **3.** Thanks to the footbridge, get the representation in $\mathscr{E}$

$$\omega^{n,2} = \Pi_{EV}\, \omega^{n,1} \in \mathscr{E}$$

- **4.** Compute $\omega^{n,3} \in \mathscr{E}$ solution at time $t^n + \Delta t_n$ of Equation (7) with the initial data $\omega^{n,2} \in \mathscr{E}$.
- **5.** Thanks to the inverse footbridge Π_{VE}, go back to the representation of the solution in $\mathscr{V}$

$$\omega^{n+1} = \Pi_{VE}\, \omega^{n,3} \in \mathscr{V}$$

- **6.** Except you reach computational final time, go to step 2.

It is clear that this algorithm involves too much numerical viscosity, in particular when $\nu = 0$. Indeed, this comes from the fact that $\Pi_{VE} \circ \Pi_{EV} \neq \mathrm{Id}_{\mathscr{V}}$.

3. A MORE RELEVANT FOOTBRIDGE

Since the L^2 projection on the finite volume space Π_{VE} introduces a too large amount of diffusion, we propose in this section to re-define an inverse footbridge. To do so, we come back to the definition of the direct footbridge (by considering Equation (2)) and we look for the existence of a right inverse of Π_{VE} in order to have zero diffusion in case of an inviscid problem. It leads us to a least square formulation and to a footbridge Π that does not present such a disadvantage. We then study the possibility of its computation. The superscripts FV and FE are used to define the space in which the function belongs.

Let u^{FE} be given in $\mathscr{E}$, we would like to find, if it exists, a function $v^{FV} = \Pi u^{FE}$ in $\mathscr{V}$ such that

$$\int_\Omega v^{FV} \varphi_j \, \mathrm{d}x = \int_\Omega u^{FE} \varphi_j \, \mathrm{d}x, \quad j = 1, \ldots, NF \tag{10}$$

Proposition 1
Assuming that (10) has a solution for all u^{FE} in $\mathscr{E}$, we have $\Pi \circ \Pi_{EV} = \mathrm{Id}_{\mathscr{V}}$.

Proof
We notice that if $v \in \mathscr{V}$ then $u^{FE} = \Pi_{EV} v$ is found by solving formula (2)

$$\int_\Omega (u^{FE} - v) \varphi_j \, \mathrm{d}x = 0, \quad \forall j = 1, \ldots, NF$$

Combining this latter equation with (10), one gets for $v^{FV} = \Pi\, u^{FE} = \Pi \circ \Pi_{EV}(v)$ the relation

$$\int_{\Omega} (v^{FV} - v)\varphi_j \, \mathrm{d}x = 0, \quad \forall j = 1, \ldots, NF \tag{11}$$

It follows that if $T_\alpha \cup T_\beta$ is the support of φ_j, then (11) becomes

$$|T_\alpha|(v_\alpha^{FV} - v_\alpha) + |T_\beta|(v_\beta^{FV} - v_\beta) = 0$$

since the function $\zeta = (v^{FV} - v)\varphi_j$ is linear on each triangle and the quadrature formula $\int_{T_\gamma} \zeta \, \mathrm{d}x = |T_\gamma| \zeta(G_\gamma)$, where G_γ is the centroid of T_γ, is exact in two dimensions.

Let us start from a boundary edge, $A_j = T_\gamma \cap \partial\Omega$. Hence, Equation (11) yields

$$|T_\gamma|(v_\gamma^{FV} - v_\gamma) = 0$$

then one has $v^{FV} = v$ on the 'boundary triangle' T_γ. Since there is no remote triangle, we conclude by induction on the next triangles: $v^{FV} = v$. □

Proposition 2
The footbridge Π_{EV} is injective.

Proof
This follows directly from the proof of Proposition 1. □

Now we are interested in the existence and computation of v^{FV} solution to (10). In order to solve this problem, we introduce the following matrix notations:

- b^{FE} is the vector of $\mathbb{R}^{NF}$ with $b_j^{FE} = \int_\Omega u^{FE}\varphi_j \, \mathrm{d}x$, $j = 1, \ldots, NF$
- B is the NF by NE real matrix with $B_{j\alpha} = \int_\Omega \chi_\alpha \varphi_j \, \mathrm{d}x$

Then (10) can be used to find the $v^{FV} \in \mathbb{R}^{NE}$ solution of the overdetermined (at least for large NE) linear system of equations

$$Bv^{FV} = b^{FE} \tag{12}$$

In general, there is no solution to system (12) except if b^{FE} belongs to the image of B. So, we consider the solution in the least squares sense

$$\text{find } v^{FV} \in \mathscr{V} \text{ such that } \|Bv^{FV} - b^{FE}\| \text{ is minimal} \tag{13}$$

This problem has one and only one solution if the rank of B is equal to the number of column, i.e. $Rk(B) = NE$ and in that case the solution is given by

$$v^{FV} = ({}^tBB)^{-1\,t}Bb^{FE}$$

We recall that Bv^{FV} is the orthogonal projection of b^{FE} on the image of B and that if $Rk(B) = NE$, then ${}^tBB$ is a symmetric, definite, positive matrix.

Proposition 3
Rank of B is equal to NE.

Proof
The proof has already been done since if one has a linear combination of the columns of B equal to zero then it is equivalent to $Bx = 0$, meaning $\Pi_{EV} x = 0$ and then $x = 0$ from Proposition 2. □

Theorem and definition
Let u^{FE} be given in $\mathscr{E}$. The mapping P_{VE}, which transforms the function u^{FE} into $v^{FV} \equiv P_{VE} u^{FE}$ in $\mathscr{V}$, a solution to (13) satisfies

$$P_{VE} \circ \Pi_{EV} = \mathrm{Id}_{\mathscr{V}}$$

Proof
It follows from Propositions 1 and 3 since the solution of the minimization problem (13) is unique. □

We now emphasize the structure of matrices B and ${}^tBB$. The matrix B has at most two non-zero coefficients per row and three per column. Indeed, on one hand if $j \in \{1, \ldots, NF\}$ is such that the edge $A_j = T_\alpha \cap T_\beta$, then

$$B_{j\gamma} = \frac{|T_\gamma|}{3} \quad \text{if } \gamma \in \{\alpha, \beta\} \quad \text{and} \quad 0 \text{ elsewhere}$$

On the other hand, if $A_j = T_\alpha \cap \partial\Omega$, one gets the following result:

$$B_{j\gamma} = \frac{|T_\gamma|}{3} \quad \text{if } \gamma = \alpha \quad \text{and} \quad 0 \text{ elsewhere}$$

Proposition 4
The matrix ${}^tBB$ is sparse.

Proof
For all triangles T_α and T_β triangles, one gets

$$({}^tBB)_{\alpha\beta} = \sum_{j=1}^{NF} B_{j\alpha} B_{j\beta} = \sum_{j=1}^{NF} \int_\Omega \chi_\alpha \varphi_j \, \mathrm{d}x \int_\Omega \chi_\beta \varphi_j \, \mathrm{d}x = \sum_{\substack{j=1 \\ j \in T_\alpha \cap T_\beta}}^{NF} B_{j\alpha} B_{j\beta} = \sum_{\substack{j=1 \\ j \in T_\alpha \cap T_\beta}}^{NF} \frac{|T_\alpha||T_\beta|}{9}$$

since $B_{j\alpha} = 0$ if the edge j does not belong to T_α.

Finally, ${}^tBB$ is given by the formula

$$\begin{cases} ({}^tBB)_{\alpha,\alpha} = \dfrac{|T_\alpha|^2}{3}, \quad \forall \alpha = 1, \ldots, NE \\ ({}^tBB)_{\alpha,\beta} = \dfrac{|T_\alpha||T_\beta|}{9} \quad \text{if } T_\alpha \neq T_\beta \text{ have a same edge} \\ ({}^tBB)_{\alpha,\beta} = 0 \quad \text{if } T_\alpha \text{ and } T_\beta \text{ do not have a common edge} \end{cases} \tag{14}$$

We proceed by showing how to compute the footbridge P_{VE}. The inversion of ${}^tBB$ is done thanks to a Choleski decomposition (once and for all for a fixed mesh) with a reordering of the rows and columns using the minimum degree algorithm (described in George and Liu [35]). Then one gets

$${}^tBB = {}^tUDU$$

where U is an upper triangular matrix with coefficient 1 on the main diagonal and D is a diagonal matrix. The computation of P_{VE} requires $O(NE^2)$ operations once the Choleski factorization has been done ($O(NE^2)$ operations).

4. ABOUT THE CANCELATION OF MESS ERRORS

We are concerned in conservation law problems: an interesting issue in this type of problem is conservation of 'mass', i.e. the integral $\int_\Omega u \, dx$, where u is the computed solution. In this section, we observe that the inverse footbridge introduces non-physical errors and we are motivated in finding a way to conserve this integral. The idea developed here consists of imposing the value of the mass to the inverse operator and leads to a constrained optimization problem which is studied. First let us show the following proposition:

Proposition 5
For all $u^{FV} \in \mathscr{V}$, $u^{FE} = \Pi_{EV} u^{FV}$ satisfies

$$\int_\Omega u^{FE} \, dx = \int_\Omega u^{FV} \, dx$$

Proof
The constant function 1 belongs to $\mathscr{E}$ since $1 = \Sigma_{j=1}^{NF} \varphi_j$. We then obtain the result by using the definition (see formula (2)) of Π_{EV}. □

On the other hand, P_{VE} does not necessarily satisfy the following property:

$$\forall u^{FE} \in \mathscr{E}, \quad \int_\Omega P_{VE} u^{FE} dx = \int_\Omega u^{FE} \, dx$$

Here is a counterexample. Let us consider the domain Ω composed by three triangles as illustrated in Figure 1. One has $NF = 7$, $NE = 3$.

Let us denote by $b_j^{FE} = \int_\Omega u^{FE}\varphi_j \, dx$ for $j = 1, \ldots, 9$. The vector $v^{FV} = P_{VE}u^{FE}$ is the solution to the system ${}^tBBv^{FV} = {}^tBb^{FE}$, which using

$$({}^tB)_{\alpha j} = \int_\Omega \chi_\alpha \varphi_j \, dx, \quad j = 1, \ldots, NF, \quad \alpha = 1, \ldots, NE$$

is equivalent to

$$\int_\Omega \chi_\alpha \sum_{j=1}^{NF} (B\, v^{FV})_j \varphi_j \, dx = \int_\Omega \chi_\alpha \sum_{j=1}^{NF} b_j^{FE}\varphi_j \, dx, \quad \alpha = 1, \ldots, NE$$

Since $\int_\Omega \chi_\alpha \varphi_j \, dx = 0$, if $j \notin T_\alpha$ one gets

$$\sum_{j \in T_\alpha} (Bv^{FV})_j \int_\Omega \chi_\alpha \varphi_j \, dx = \sum_{j \in T_\alpha} b_j^{FE} \int_\Omega \chi_\alpha \varphi_j \, dx, \quad \alpha = 1, \ldots, NE$$

and it yields

$$\sum_{j \in T_\alpha} (Bv^{FV})_j = \sum_{j \in T_\alpha} b_j^{FE}$$

In the present case, we obtain the following system for the three components v_α^{FV}:

$$\begin{cases} |T_1| v_1^{FV} + \dfrac{|T_2|}{3} v_2^{FV} = b_1^{FE} + b_2^{FE} + b_3^{FE} \\ |T_2| v_2^{FV} + \dfrac{|T_1|}{3} v_1^{FV} + \dfrac{|T_3|}{3} v_3^{FV} = b_3^{FE} + b_4^{EF} + b_5^{FE} \\ |T_3| v_3^{FV} + \dfrac{|T_2|}{3} v_2^{FV} = b_5^{FE} + b_6^{FE} + b_7^{FE} \end{cases}$$

It is then straightforward that

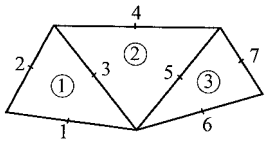

Figure 1. 3-triangle domain.

$$\int_\Omega v^{FV}\,\mathrm{d}x = \sum_{\alpha=1}^{3} |T_\alpha| u_\alpha^{FV} = \frac{1}{7}(6b_1^{FE} + 6b_2^{FE} + 9b_3^{FE} + 3b_4^{FE} + 9b_5^{FE} + 6b_6^{FE} + 6b_7^{FE})$$

which is different (for almost all the values) from $\int_\Omega u^{FE}\,\mathrm{d}x = \Sigma_{j=1}^{7} b_j^{FE}$. □

We propose to modify the footbridge P_{VE} in such a way that it will conserve $\int_\Omega u\,\mathrm{d}x$ and still follows $P_{VE} \circ \Pi_{EV} = \mathrm{Id}_{\mathscr{V}}$.

So we replace problem (13) by the following constrained optimization problem:

$$\begin{cases} \text{find } v^{FV} \in \mathscr{V} \text{ minimizing } \|Bv^{FV} - b^{FE}\| \\ \text{under the constraint } \displaystyle\int_\Omega v^{FV}\,\mathrm{d}x = \sum_{j=1}^{NE} b_j^{FE} \end{cases} \tag{15}$$

Let us denote $m = \Sigma_{j=1}^{NF} b_j^{FE}$ and $C = {}^t(|T_1|, \ldots, |T_{NE}|)$ the vector of $\mathbb{R}^{NE}$ whom components are the triangle areas. The constraint may be then written as

$${}^tCv^{FV} = m$$

Hence using the Lagrange multiplier method, the constrained condition is included implicitly in the formulation that now involves a saddle-point problem

$$\begin{cases} \text{find } (v^{FV}, \lambda) \in \mathscr{V} \times \mathbb{R} \\ \text{that make stationary } \phi(v^{FV}, \lambda) = \|Bv^{FV} - b^{FE}\|^2 + 2({}^tCv^{FV} - m)\lambda \end{cases} \tag{16}$$

It is well known that if $(v_*^{FV}, \lambda_*) \in \mathscr{V} \times \mathbb{R}$ is a saddle-point of ϕ, i.e.

$$\phi(v_*^{FV}, \lambda) \le \phi(v_*^{FV}, \lambda_*) \le \phi(v^{FV}, \lambda_*), \quad \forall \lambda \in \mathbb{R} \quad \text{and} \quad \forall u^{FV} \in \mathscr{V}$$

then v_*^{FV} is a solution to problem (16).

Furthermore, one has

$$\frac{\partial \phi}{\partial v^{FV}}(v_*^{FV}, \lambda_*) = 0, \qquad \frac{\partial \phi}{\partial \lambda}(v_*^{FV}, \lambda_*) = 0$$

meaning that (v_*^{FV}, λ_*) is the solution of the linear system

$$\begin{pmatrix} {}^tBB & C \\ {}^tC & 0 \end{pmatrix} \begin{pmatrix} v_*^{FV} \\ \lambda_* \end{pmatrix} = \begin{pmatrix} {}^tBb^{FE} \\ m \end{pmatrix} \tag{17}$$

Conversely, considering $v_*^{FV} \in \mathscr{V}$ solution of (16) and let

$$\lambda_* = -\frac{(BC,\, Bv_*^{FV} - b^{FE})}{\|C\|^2}$$

then (v_*^{FV}, λ_*) is a saddle-point of ϕ.

The matrix

$$\begin{pmatrix} {}^tBB & C \\ {}^tC & 0 \end{pmatrix}$$

is invertible since ${}^tBB$ is a positive-definite matrix and ${}^tC({}^tBB)^{-1}C$ is different from zero. Then, problem (16) has a unique solution, which allows us to construct another footbridge P_{VE}^* as follows. Let u^{FE} be given in $\mathscr{E}$, then the application P_{VE}^*, which associates with u^{FE} the element $v_*^{FV} = P_{VE}^* u^{FE} \in \mathscr{V}$, a solution of (17), satisfies

- $P_{VE}^* \circ \Pi_{EV} = \mathrm{Id}_{\mathscr{V}}$
- $\int_\Omega P_{VE}^* u^{FE}\, \mathrm{d}x = \int_\Omega u^{FE}\, \mathrm{d}x, \quad \forall u^{FE} \in \mathscr{E}$

The scheme for implementing the footbridge P_{VE}^* is now described. A block factorization is computed to solve system (17). Since ${}^tBB$ is factorized in the form

$${}^tBB = {}^tUDU$$

we expect that the factorization of (17) may be written as

$$M = \begin{pmatrix} {}^tBB & C \\ {}^tC & 0 \end{pmatrix} = \begin{pmatrix} {}^tU & 0 \\ {}^tS & 1 \end{pmatrix} \begin{pmatrix} D & 0 \\ 0 & H \end{pmatrix} \begin{pmatrix} U & S \\ 0 & 1 \end{pmatrix}$$

A simple substitution gives

$$M = \begin{pmatrix} {}^tUDU & {}^tUDS \\ {}^tSDU & H + {}^tSDS \end{pmatrix}$$

and hence

$$S = D^{-1}{}^tU^{-1}C, \qquad H = -{}^tSDS$$

Since D and U are invertible, S is a vector of $\mathbb{R}^{NE}$ different from zero and H belongs to $\mathbb{R}^*$. So the computation of this footbridge requires no further operations.

5. A TWO-DIMENSIONAL SCALAR CONVECTION–DIFFUSION EQUATION

The first series of numerical experiments performed to test the scheme described in previous sections concerns the approximation of the solution to the initial value problem (5) over the domain $\Omega =]0, 3[\times]0, 3[$, with the following boundary conditions:

$$\frac{\partial \omega}{\partial y}(x, \pm 3) = 0, \quad \text{i.e. Neumann conditions}$$

and

$$\omega(0, y) = \omega(3, y) \quad \text{i.e. periodic conditions}$$

These conditions are formulated in such a way that they are well suited to each of the fractional steps (6) and (7). Note that for this particular problem, the exact solution ω is such that the integral $\int_\Omega \omega \, dx$ remains constant in time.

The initial condition for all simulations considered here corresponds to a Gaussian cone at position $x = 0.5$ and $y = 1.5$ and is given by

$$\omega_0(x, y) = \exp(-50((x - 0.5)^2 + (y - 1.5)^2))$$

We expect that our discrete scheme for the diffusive part provides good approximations of the solutions for large Peclet numbers (where the Peclet number $Pe = \|C\|h/\nu$ measures the ratio between convective effects and diffusive effects) and is not sensitive to the size of Pe. However, we are aware that simulations also depend of the approximation of each step, and in particular that the convective scheme may involve too much viscosity. To examine these properties, we consider two different kinds of advection.

5.1. An advection parallel to the mesh

5.1.1. Results with the footbridge defined in Section 4. The domain is discretized into three grids similar to the regular Cartesian mesh show in Figure 2 with, respectively, $2 \times 30 \times 30$, $2 \times 60 \times 60$, $2 \times 120 \times 120$ triangles. The convection vector C is equal to $(1/2, 0)$ and tests are done with six values of the viscosity coefficient varying from 0 to 10^{-1}. For ν smaller than 10^{-3}, i.e. Peclet number larger than 12.5, we have a regime dominated by convection. For ν equal to 10^{-2}, the Peclet number is around 5: convective and diffusive effects are similar. For ν equal to 10^{-1}, we have a regime dominated by diffusion with a Peclet number less than 1.

The time step is chosen according to stability conditions: it must enforce the Courant–Friedrich–Lewy (CFL) condition for the convective step. In others words, Δt is computed in such a way that the following CFL number is less than or equal to 1 ($\vec{v}_j$ denotes the unit normal vector to the edge A_j)

$$\mathrm{CFL} \equiv \max_{T_\alpha \in \mathscr{T}} \max_{A_j \in \partial T_\alpha} \Delta t \frac{|A_j| |C \cdot \vec{v}_j|}{|T_\alpha|} \tag{18}$$

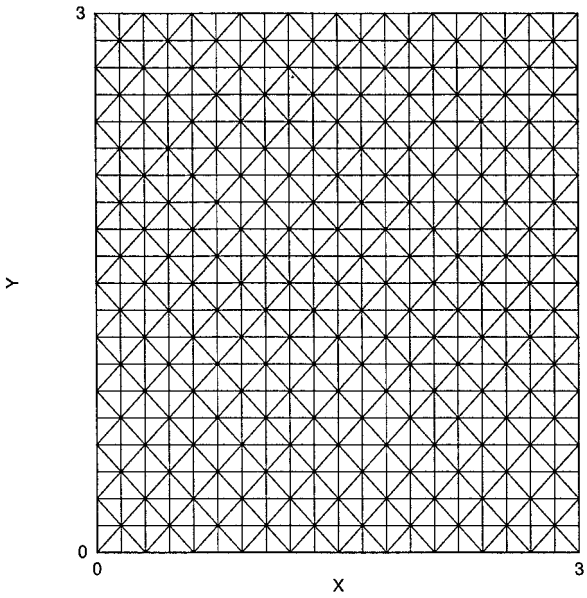

Figure 2. Regular mesh of $20 \times 20 \times 2$ triangles.

For the present regular meshes, the CFL number is exactly 1 for, respectively, Δt equal to 3/30, 3/60, 3/120.

We integrate the evolution equation using the numerical model defined in Section 4 between $t = 0.0$ and $t = 6.0$. The partial differential equation (5) moves the cone to the right and at final time the Gaussian cone has reached its initial position. The influence of the physical or numerical viscosity can be seen in the resulting cone height and in the shape of the computed convected cone.

At time $t = 6.0$, cuts through the field ω at position $x = 0.5$ and $y = 1.5$ are shown in Figures 3–8 (the field has been post-processed: the cell values are projected on the nodes of the mesh). These cuts allow a qualitative comparison of the simulations obtained with different values of the parameter v. In case of a zero parameter, simulations reproduce exactly the field ω at time $t = 6.0$ without any numerical diffusion since horizontal and vertical profiles are similar to the initial ones. This result conforms with the building of the footbridges and the property $P^*_{VE} \circ \Pi_{EV} = \mathrm{Id}_{\mathcal{V}}$. For $v = 10^{-5}$ and 10^{-4}, the height of the cone decreases slowly with time, which is due to the low viscosity parameter. With $v = 10^{-2}$ and 10^{-1}, the method we present reproduces the effect of the diffusive operator very precisely (low height and stretch shape of the cone) and retains the correct value of $\int_\Omega \omega \, \mathrm{d}x$ since the errors produced on it are very similar to the epsilon machine during all the time evolution. These results are mostly independent of the refinement level of the mesh.

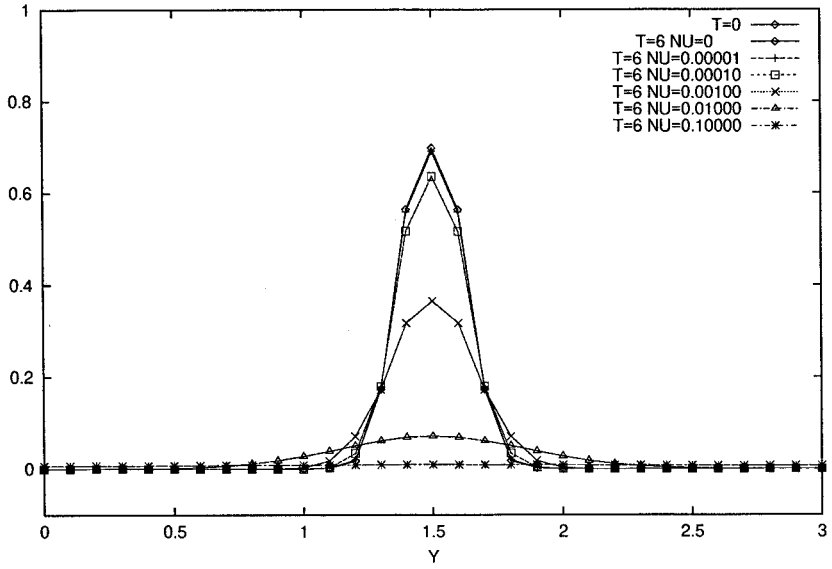

Figure 3. Mesh 30×30: cut at $X = 0.5$ at $t = 6.0$.

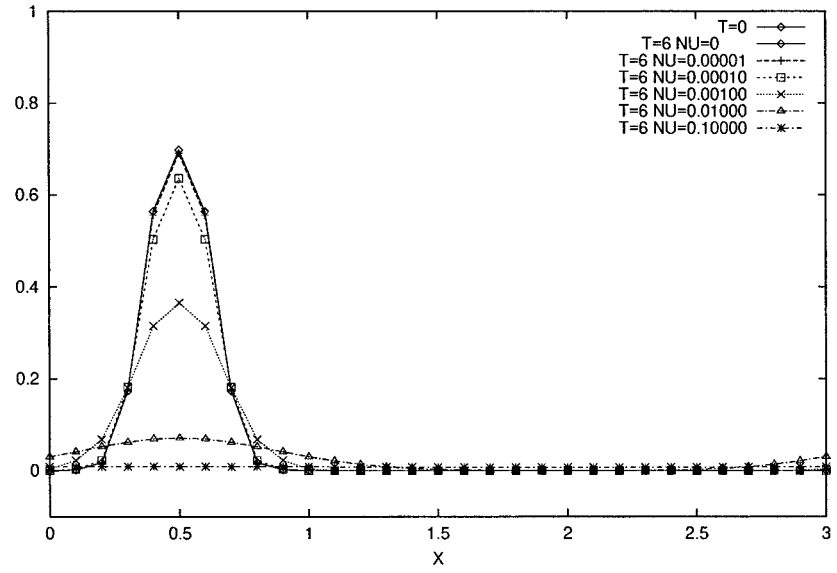

Figure 4. Mesh 30×30: cut at $Y = 1.5$ at $t = 6.0$.

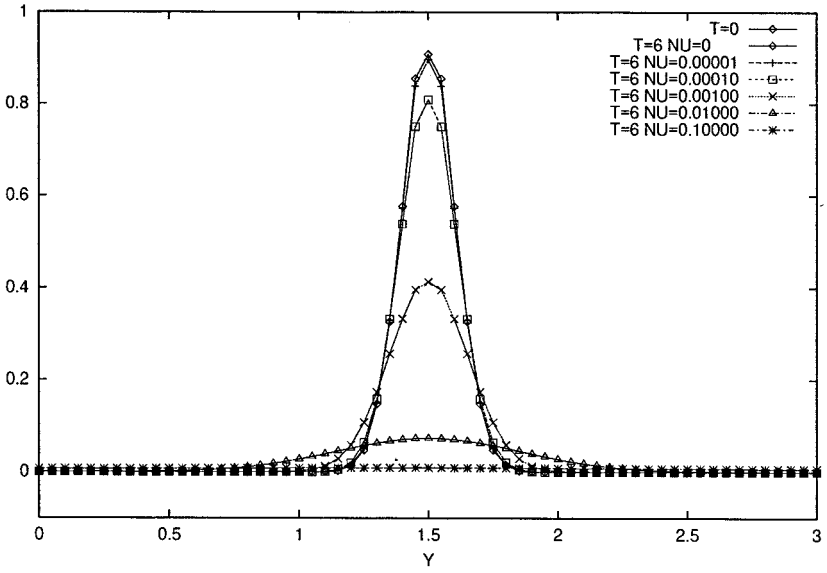

Figure 5. Mesh 60×60: cut at $X = 0.5$ at $t = 6.0$.

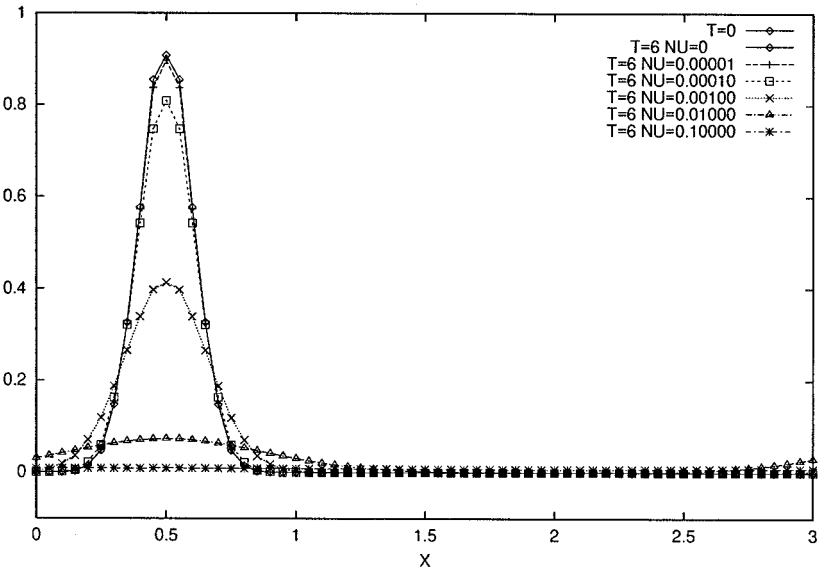

Figure 6. Mesh 60×60: cut at $Y = 1.5$ at $t = 6.0$.

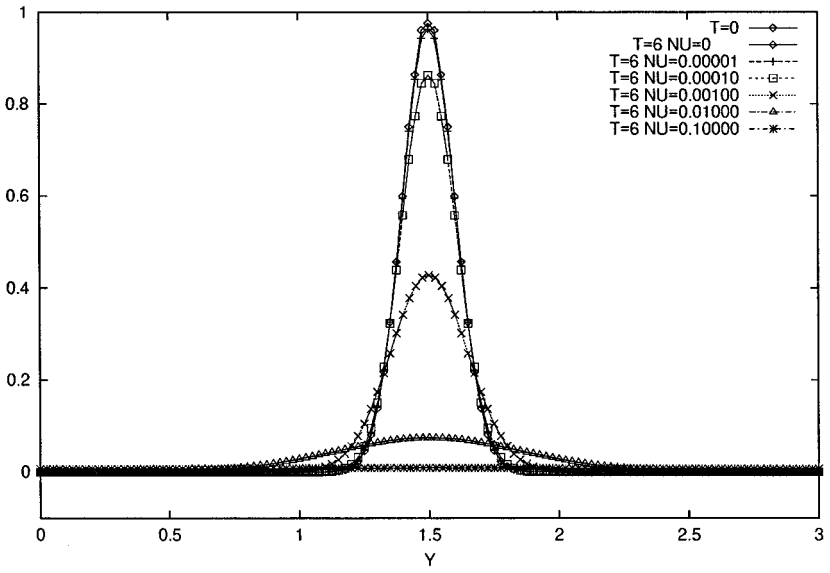

Figure 7. Mesh 120×120: cut at $X = 0.5$ at $t = 6.0$.

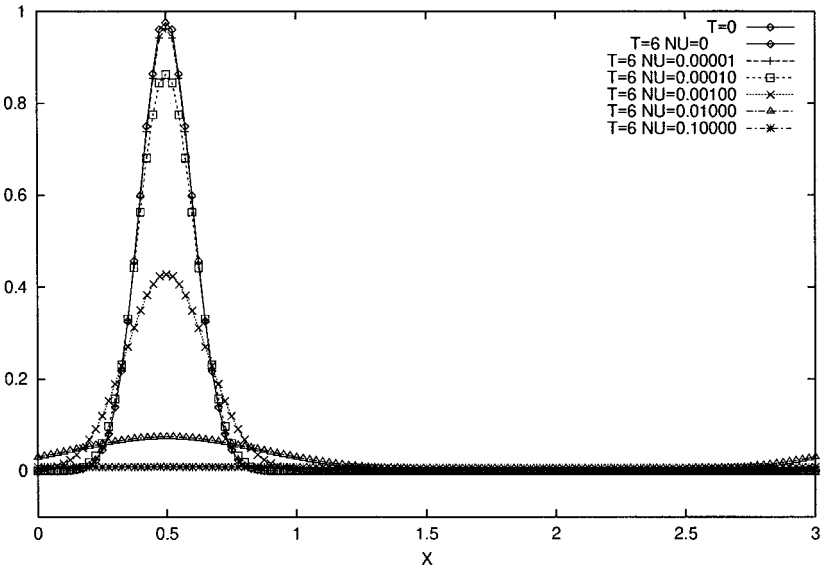

Figure 8. Mesh 120×120: cut at $Y = 1.5$ at $t = 6.0$.

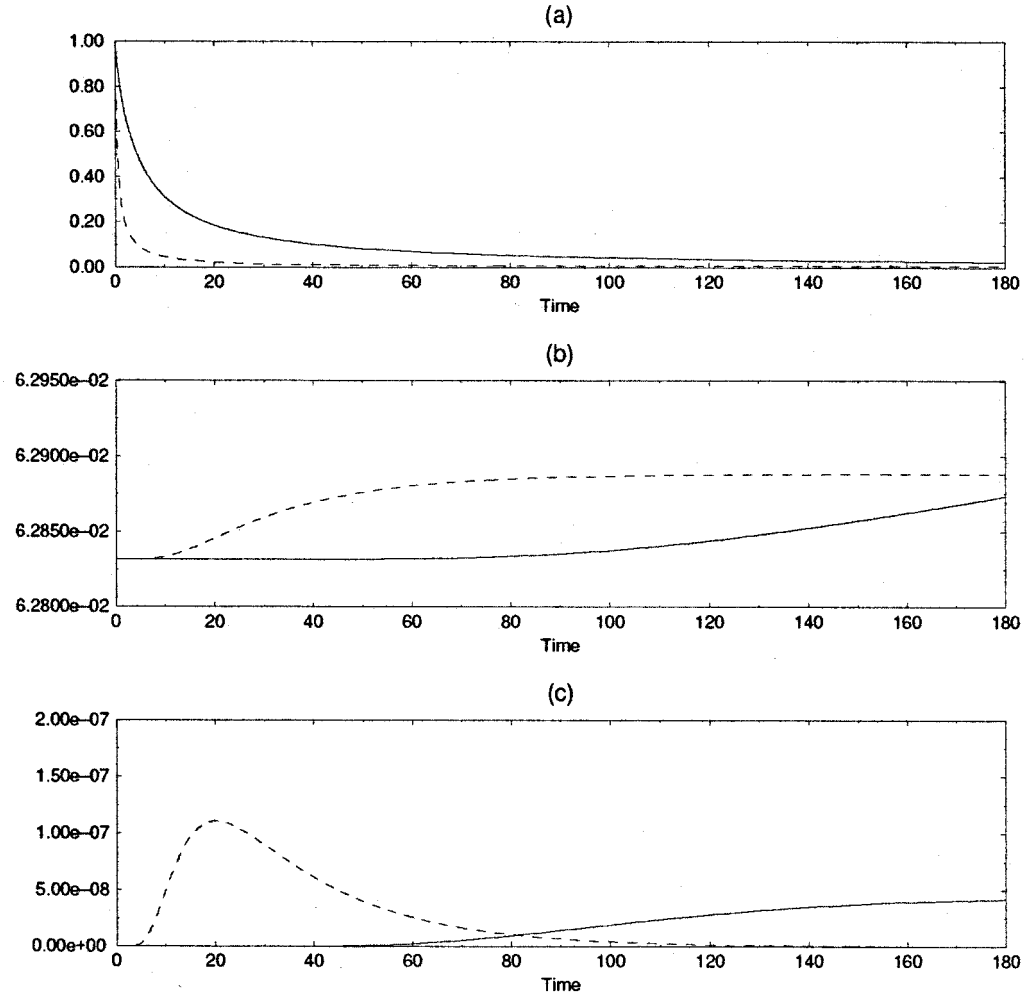

Figure 9. Mesh 40×40. Evolution of (a) the height of the cone, (b) the mass integral, (c) the variation of the mass integral. Continuous line: $\nu = 0.001$. Dashed line: $\nu = 0.01$.

5.1.2. Studies of the operator defined in Section 3. We sum up computations with the inverse footbridge defined in Section 3 and on an intermediate mesh of $2 \times 40 \times 40$ triangles. Since it does not cancel errors in $\int_\Omega \omega \, dx$, the simulations of this integral present slightly small non-monotonically errors in time. Indeed, Figure 9 shows the evolution of (a) the maximum of the finite volume solution (which corresponds to the height of the cone and which still behaves corectly) but also of (b) $\int_\Omega \omega^{FV} dx$ and (c) its variation during the longer time interval [0, 180]. One can notice that the values of $\int_\Omega \omega^{FV} dx$, which depend on the topology of the

mesh (there are some regular triangulations of Ω for which the inverse footbridge defined in Section 3 cancels the errors on it) do not differ so much from the initial value. It can be observed in Figure 9(b) that there is a slight increase but less than 0.1 per cent at $t = 180.0$ and on Figure 9(c) that at each time step, the increase stay below 10^{-7}. Table I, which gives the numerical values of the integral at the beginning and at the end of the computation, confirms this small increase (at least for viscous parameter larger than 10^{-3}) but suggests that this constraint on cancelling errors in $\int_\Omega \omega \, dx$ is not very important in the present case.

5.1.3. Comparison with an overkilled solution. Now we describe some numerical results of convergence in order to validate the algorithm. A measurement of the numerical convergence has to be defined. Since there is no analytical solution to the problem (even for this simple linear problem), one way to measure the convergence is to compare the results with an 'overkilled' solution u^{Ref} of the problem, i.e. a considered as exact solution which is computed at time $t = 6.0$ on a very fine mesh with a converging known scheme. In the present case, a classical upwind finite difference semi-implicit scheme is employed to approximate the solution on a regular mesh of 1000×1000 points, with the CFL number equal to 1.

In Figure 10 for the parameter $v = 0.001$ and in Figure 11 for a lower viscous parameter $v = 0.00001$, we have plotted (with a log–log scale) versus the space step h (we take $h = 3/n$ for the $2 \times n \times n$ triangles mesh) the following data:

- the maximum of the overkilled solution u^{Ref} (continuous line)
- the maximum of the computed solution u^{VF} (crosses points)
- the L^∞ difference $\max_\Omega (|u^{VF} - u^{\mathrm{Ref}}|)$ (diamond points)
- the L^2 difference $\dfrac{1}{|\Omega|}\left(\int_\Omega (u^{VF} - u^{\mathrm{Ref}})^2 \, dx\right)^{1/2}$ (square points)
- the L^1 difference $\dfrac{1}{|\Omega|}\int_\Omega |u^{VF} - u^{\mathrm{Ref}}| \, dx$ (plus points)
- the reference slope -1 with a dash line

In both cases, one can observe that the maximum of the computed solution u^{VF} converges to the maximum of the overkilled solution and that the rate of convergence of the three differences is governed by the order of space step ($O(h)$), since curves are parallel to the slope -1 (at least for small h).

Table I. Errors on the mass integral.

Time	v	Mass integral mesh 40×40	% initial mass integral
180	0	0.62831841E−01	100
180	10^{-4} and 10^{-5}	0.62831841E−01	100
180	10^{-3}	0.62873417E−01	100.07
180	10^{-2}	0.62888212E−01	100.09
180	10^{-1}	0.62838604E−01	100.01

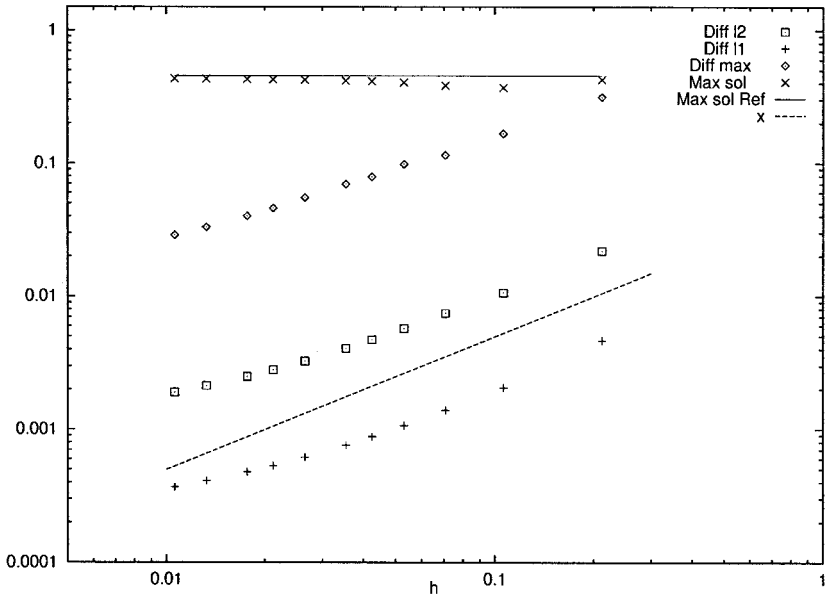

Figure 10. Comparison with an overkilled solution: differences versus space step for $v = 0.001$.

5.2. An advection non parallel to the mesh

Here we seek the solution of the same scalar convection–diffusion equation but computations are now obtained on an unstructured mesh as shown in Figure 12. From this mesh, we have performed a sequence of three finer meshes by successively dividing each triangle into 4 congruent triangles. Some further parameters like the number of volumes (NE), the number of edges (NF), the minimum and the maximum of the triangle areas are reported in Table II, where we have also listed the time step and the corresponding Peclet number. Here the time step is chosen such that the CFL given by formula (18) is equal to 1.

We have collected the initial and final height of the cone (respectively at time $t = 0.0$ and at time $t = 6.0$) in Table III and computed the ratio between these two values. One can notice that in the present case, the advective fractional step does not accurately convect the Gaussian cone in the sense that its shape is widely stretch at final time even for a zero viscous parameter. For instance, for the coarser grid, the final amplitude of the cone represents only 14.8 per cent of the initial one and in Figures 13 and 14, the final profile for $v = 0$ does not any longer compare with the initial one. This is due to the poor ability of schemes to reproduce pure convection on unstructured grid without involving too much viscosity and specially, like it is the case here, with low-order and explicit scheme. These distortions with the initial cone decrease when the grid becomes finer.

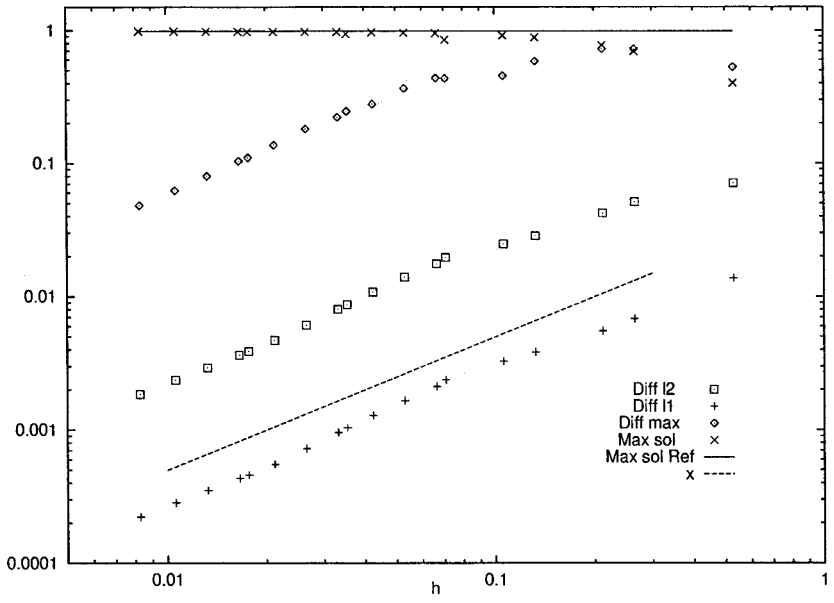

Figure 11. Comparison with an overkilled solution: differences versus space step for $v = 0.00001$.

Nevertheless, cuts through the solution field at $t = 6.0$ shown in Figures 13 and 14 and the behavior of the height of the bump with the viscous parameter in Table III confirm the observation that the footbridges and splitting operators have a good ability to discretize the diffusive operator in the cell finite volume context. Indeed, on one hand as long as the convective step involves too much viscosity, final results are not changes, i.e. no more diffusion is added to the computation, and on the other hand in a dominant diffusive regime, results correspond to the expected ones: the physical diffusion decreases and spreads the cone and the phenomena are independent of the mesh. At this stage, we must emphasize that the slightly deformed shape of the resulting cone is artificial and is due to the graphical process we choose to represent a piecewise constant function without any post-processed projection on the nodes.

6. A NON-LINEAR SYSTEM

In this section, we present numerical results that demonstrate the performance of the footbridges between finite volume representation and finite volume element representation introduced to discretized diffusion operators in the case of more complex two-dimensional models. All the numerical examples proposed here refer to the inverse footbridge P^*_{VE} described in Section 4.

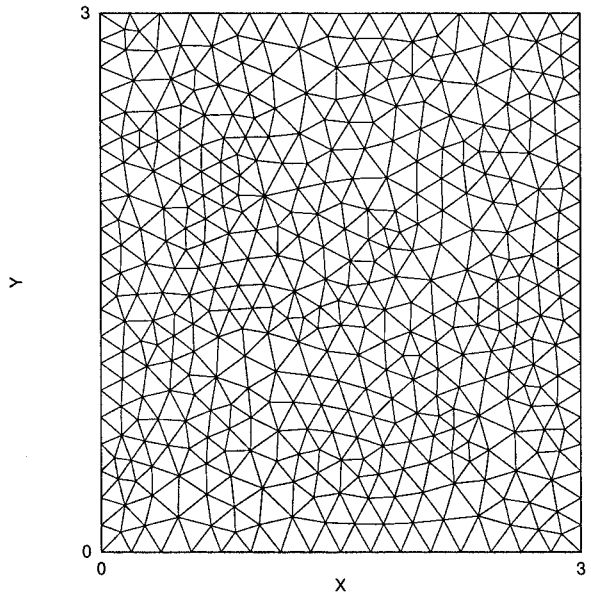

Figure 12. The coarse mesh.

Table II. Non-parallel mesh advection: parameters of the meshes.

	Grid 1	Grid 2	Grid 3
NE	3112	12 448	49 792
NF	4740	18 816	74 976
$\min \lvert T \rvert$	0.00108	0.00027	0.000058
$\max \lvert T \rvert$	0.00670	0.001675	0.00041875
Δt	0.0425	0.02125	0.010625
Peclet number	$0.06217/\nu$	$0.03108/\nu$	$0.01554/\nu$

6.1. A system from gas dynamics

We consider a simplified model of the Navier–Stokes equations. The non-linear system, which models compressible and isentropic flows, is given by

$$\frac{\partial}{\partial t}\begin{pmatrix}\varrho\\ \varrho\omega\end{pmatrix}+\nabla\cdot\begin{pmatrix}\varrho\omega\\ \varrho\omega\otimes\omega+p\,\mathrm{Id}\end{pmatrix}-\nabla\cdot\begin{pmatrix}0\\ \mathscr{T}\end{pmatrix}=0 \tag{19}$$

We note ϱ as the density and ω as the velocity field ${}^t(u, v)$. The pressure p follows $p=\varrho^{\gamma}$ and the viscous tensor $\mathscr{T}$ is defined by

Table III. Non-parallel mesh advection: maximum of the solution at $t = 6.0$ and its ratio to the maximum at $t = 0.0$.

$\max\{\omega_\alpha\}$ at $t = 0$	Grid 1 0.941	Grid 2 0.993	Grid 3 1.000
$\nu = 0$	0.139 (14.8)	0.290 (29.2)	0.446 (44.6)
$\nu = 10^{-5}$	0.139 (14.8)	0.289 (29.1)	0.444 (44.4)
$\nu = 10^{-4}$	0.137 (14.6)	0.279 (28.1)	0.421 (42.1)
$\nu = 10^{-3}$	0.117 (12.4)	0.211 (21.2)	0.285 (28.5)
$\nu = 10^{-2}$	0.0502 (5.30)	0.0635 (6.40)	0.0693 (6.93)
$\nu = 10^{-1}$	0.00818 (0.90)	0.00898 (0.90)	0.00904 (0.90)

Percentages in parentheses.

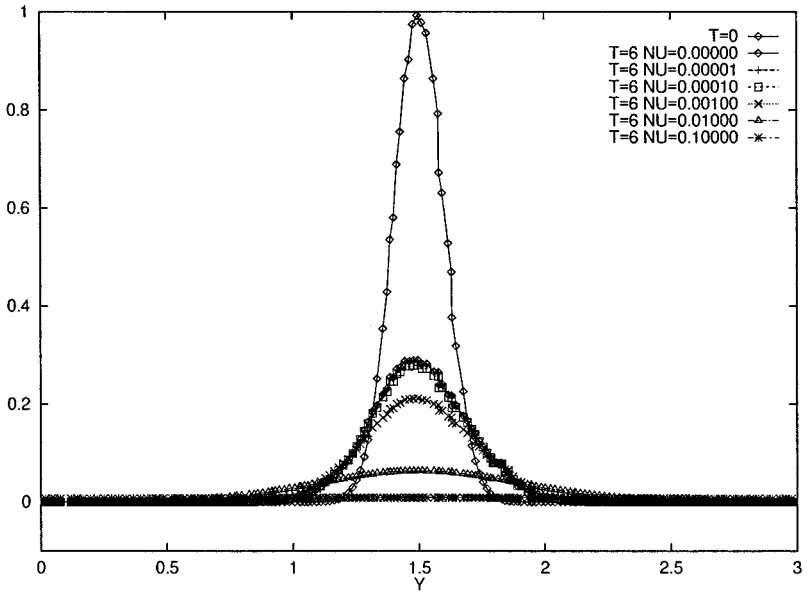

Figure 13. Grid 2: cuts at $X = 0.5$ at $t = 6.0$.

$$\mathscr{T} = \nu\left\{(\nabla\omega + {}^t\nabla\omega) - \frac{2}{3}(\nabla\cdot\omega)\mathrm{Id}\right\}$$

To solve system (19), we implement the fractional technique we have described in Section 2. The first step is concerned with the Euler system of an isentropic gas and corresponds to $\mathscr{T} = 0$. It is solved by an explicit first-order accurate upwind finite volume scheme lying on the notion of characteristic flux proposed by Ghidaglia *et al.* [36]. Let us remind now how this scheme approximates the solution of the following hyperbolic system in space dimension d:

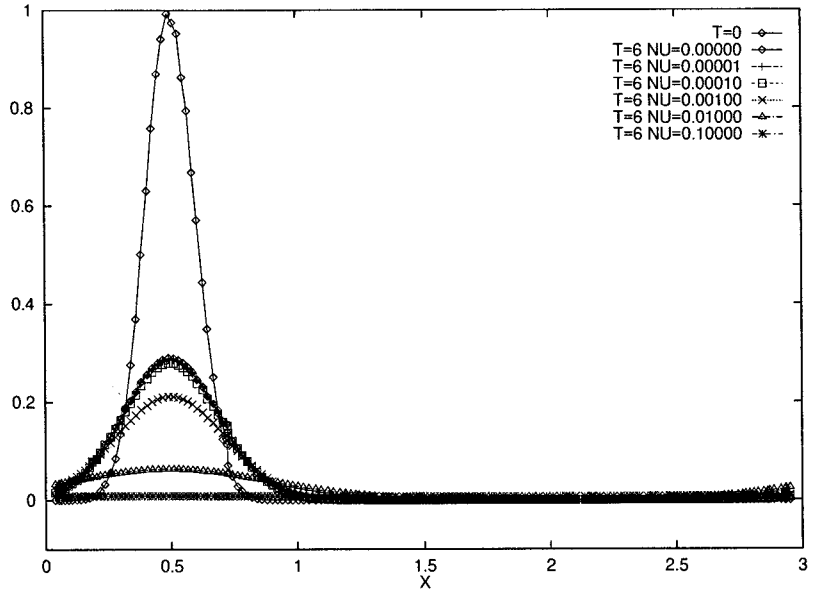

Figure 14. Grid 2: cuts at $Y = 1.5$ and $t = 6.0$.

$$\frac{\partial v}{\partial t} + \nabla \cdot f(v) = 0 \quad \text{or, similarly,} \quad \frac{\partial v}{\partial t} + \sum_{i=1}^{d} \frac{\partial f_i}{\partial x_i}(v) = 0$$

If n is a unitary vector of $\mathbb{R}^d$, we denote $A(v, n)$ the diagonalizable Jacobian matrix

$$A_{kl}(v, n) = \sum_{i=1}^{d} \frac{\partial f_i^k(v)}{\partial v_l} n_i, \quad 1 \le k, l \le d$$

and we suppose that the sign matrix is defined in the following way:

$$\operatorname{sgn}(A(v, n)) = P^{-1} \operatorname{sgn}(\operatorname{diag}(\lambda_i))P$$

where $A(v, n) = P^{-1} \operatorname{diag}(\lambda_i)P$. Here $\operatorname{diag}(\lambda_i)$ is the diagonal matrix of eigenvalues. Let K and L be two volumes such that $K \cap L \neq \varnothing$, the numerical flux function on their interface $K \cap L$ is then approximated by the characteristic flux defined by the following formulas:

$$\begin{cases} \Phi(v_K, v_L, \vec{v}_{K,L}) \equiv \dfrac{f(v_K) + f(v_L)}{2} \cdot \vec{v}_{K,L} - \operatorname{sgn}(A(\mu_{K,L}, \vec{v}_{K,L})) \cdot \left(\dfrac{f(v_L) - f(v_K)}{2} \cdot \vec{v}_{K,L} \right) \\ \mu_{K,L} = \dfrac{|K| v_K + |L| v_L}{|K| + |L|} \end{cases} \tag{20}$$

where $\vec{v}_{K,L}$ is the unit normal to $K \cap L$ oriented from K to L and v_K (resp. v_L) represents the approximation of v on K (resp. L).

Hence in the present case, if W_K^n is the approximate solution of (19) on the nth time level in the volume K, step 2 of the algorithm described in Section 2 is replaced by

$$W_K^{n+1,1} = W_K^n - \frac{\Delta t}{|K|} \sum_{L \in \mathcal{N}(K)} |K \cap L| \Phi(W_K^n, W_L^n, \vec{v}_{K,L}) \quad \forall K \in \mathcal{T}$$

This explicit step is stable under the following CFL condition:

$$\mathrm{CFL} \equiv \max_{K \in \mathcal{T}} \max_{L \in \mathcal{N}(K)} \max_i \Delta t \frac{|K \cap L| |\lambda_i|}{|K|} \leq 1 \tag{21}$$

In the second fractional step concerning the diffusion problem, i.e. step 4 of our approach, the system can be readily written as

$$\begin{cases} \dfrac{\partial \rho}{\partial t} = 0 \\ \dfrac{\partial (\rho u)}{\partial t} = v \dfrac{\partial}{\partial x} \left\{ 2 \dfrac{\partial u}{\partial x} - \dfrac{2}{3} \left(\dfrac{\partial u}{\partial x} + \dfrac{\partial v}{\partial y} \right) \right\} + v \dfrac{\partial}{\partial y} \left(\dfrac{\partial u}{\partial y} + \dfrac{\partial v}{\partial x} \right) \\ \dfrac{\partial (\rho v)}{\partial t} = v \dfrac{\partial}{\partial x} \left(\dfrac{\partial u}{\partial y} + \dfrac{\partial v}{\partial x} \right) + v \dfrac{\partial}{\partial y} \left\{ 2 \dfrac{\partial v}{\partial y} - \dfrac{2}{3} \left(\dfrac{\partial u}{\partial x} + \dfrac{\partial v}{\partial y} \right) \right\} \end{cases} \tag{22}$$

One notices that in this step $\rho(x, t) = \rho(x, t_n)$, for all $t > t^n$. Hence, the direct and the inverse footbridge (steps 3 and 5 of our approach) are applied only to the components of the velocity. Afterwards, we use a variational formulation in $\mathscr{E}^2$ to approximate the solution (u, v) of the two last equations of the system (22) with an implicit (and stable) forward Euler scheme for the time discretization.

6.2. A shock tube problem

We first provide results for an extension of the one-dimensional Sod tube, which is a standard test case for Euler solvers. Here, we consider the viscous solution of this problem. We take the unstructured mesh shown in Figure 15 and integrate over the rectangle $\Omega = [-0.5, 1.5] \times [0, 1]$ system (19), with $p = \rho^{1.4}$. The initial data are $u = v = 0$ in Ω and $\rho = 1$ for $x < 0.5$ and $\rho = 0.193$ for $x > 0.5$. To ensure the stability condition (21), we have set $\Delta t = 0.004$.

Boundary conditions at $y = 0$ and $y = 1$ are wall boundary conditions meaning $\omega \cdot \vec{v} = 0$. Some Neuman conditions are simply implemented at the outflow lateral boundaries as long as a non-zero velocity does not reach them and since we do not want to address the open compressible Navier–Stokes problem of boundary conditions at this stage. Let us define that for this particular test, boundary conditions are identical in the inviscid and viscous steps.

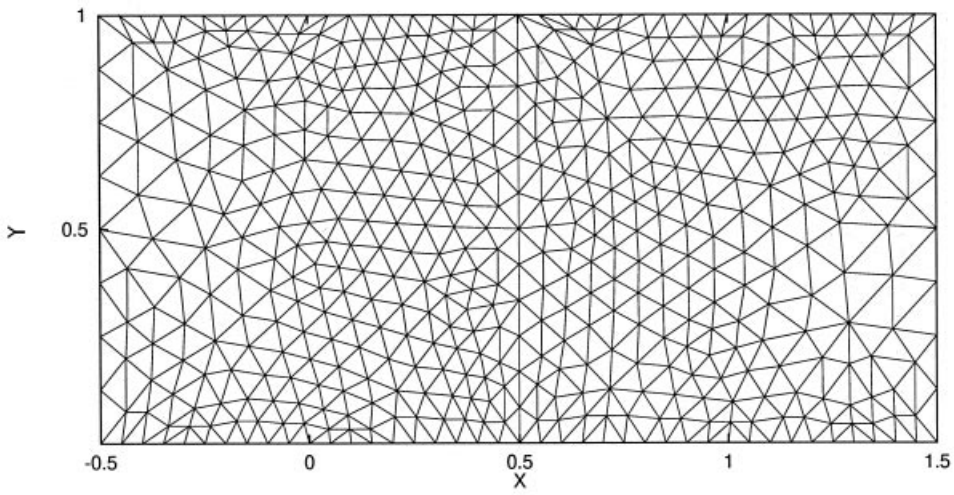

Figure 15. Mesh over the domain $[-0.5, 1.5] \times [0, 1]$.

At time $t = 0.21$, Figure 16 shows the finite volume representation of the pressure and Figure 17 the finite element representation (the mid-edge values have been joined together) of the first component of the velocity, both computed with a zero viscous parameter. The vertical component of the velocity is almost zero and cuts at constant y compare well with standard results for this problem in one dimension. Indeed, one can observe that the method resolves the dynamic of the moving rarefaction wave and shocks and that the presence of the footbridges does not modify in any sense the solution since it is built for.

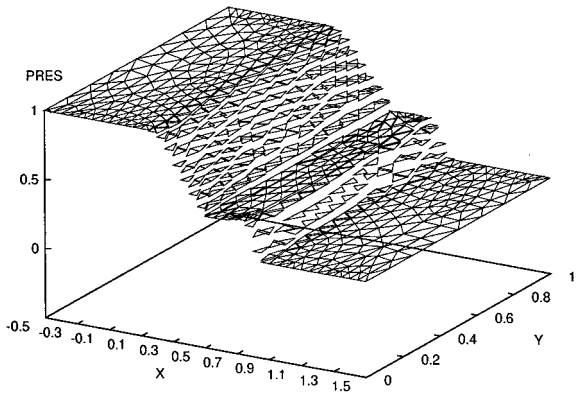

Figure 16. $v = 0$: finite volume solution of the pressure $(= \rho^{\gamma})$ at $t = 0.21$.

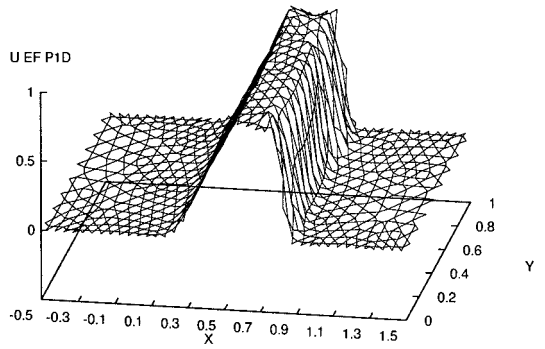

Figure 17. $v = 0$: finite element solution of horizontal velocity at $t = 0.21$.

For $v = 0.01$, looking at the finite volume representation of the pressure and the finite element representation of the horizontal velocity plotted in Figures 18 and 19, one can observe that the footbridges take into account the viscosity in a relevant way. Cuts through the horizontal axis $y = 0.26$ in the horizontal velocity field in Figure 20 and the density in Figure 21 show that the viscous terms are correctly approximated for different values of the parameter v. The continuous line curves represent the exact solution for the inviscid problem. The moving shocks are smoothed and neither the finite solution nor the finite element one present spurious oscillations.

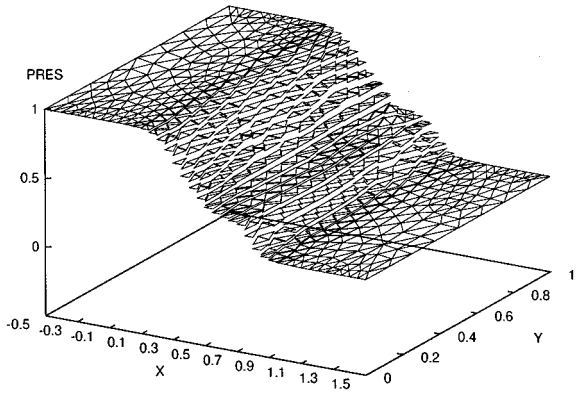

Figure 18. $v = 0.01$: finite volume solution of pressure at $t = 0.21$.

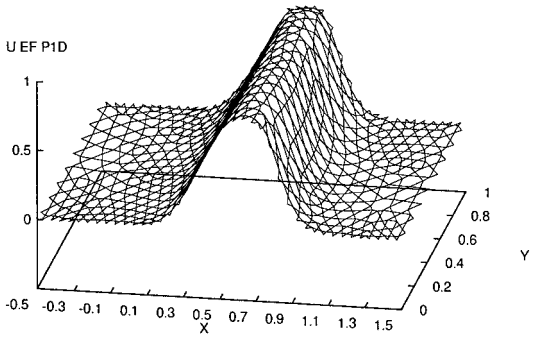

Figure 19. $v = 0.01$: finite element solution of horizontal velocity at $t = 0.21$.

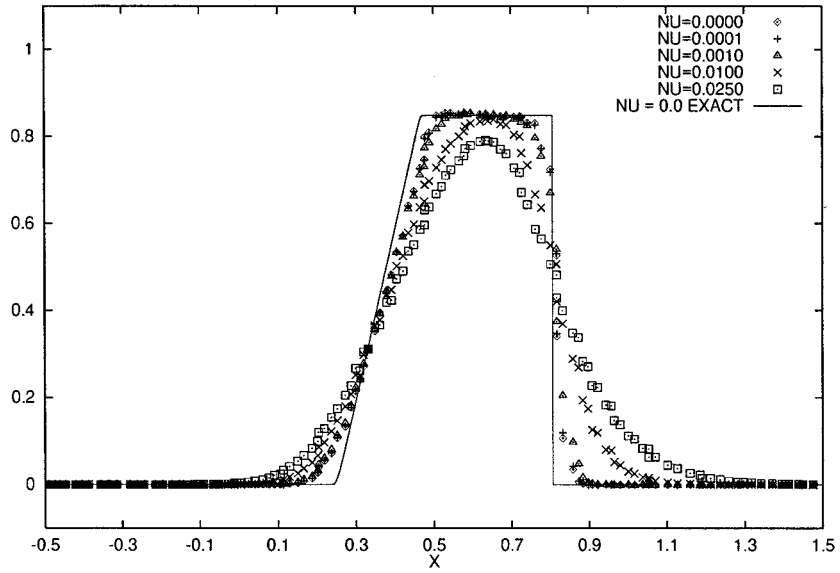

Figure 20. Cuts through the horizontal velocity at $Y = 0.26$ and $t = 0.21$ for five values of v.

6.3. Flow over a NACA0012 airfoil section

The efficiency of the proposed method is now illustrated by considering (following Glowinski and Periaux [37]) a two-dimensional viscous flow around an NACA0012 airfoil at an angle of attack of 0° and a viscous parameter equal to 0.002. We assume the flow to be uniform at infinity and the variables to be non-dimensionalized by a free stream vector. We prescribe the density ρ_∞ and the velocity $\omega_\infty = {}^t(u_\infty, 0)$ such that mach number at infinity is equal to 0.85.

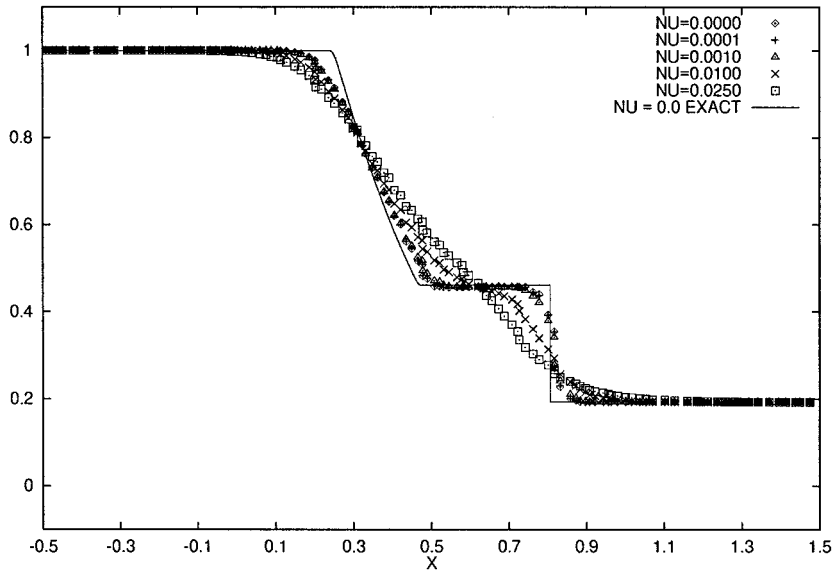

Figure 21. Cuts through the density at $Y = 0.26$ and $t = 0.21$ for five values of v.

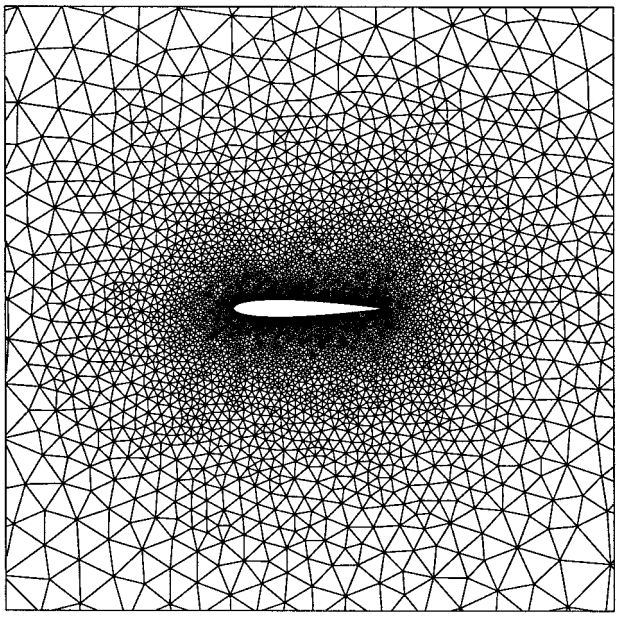

Figure 22. Detail of the grid around the NACA0012 airfoil.

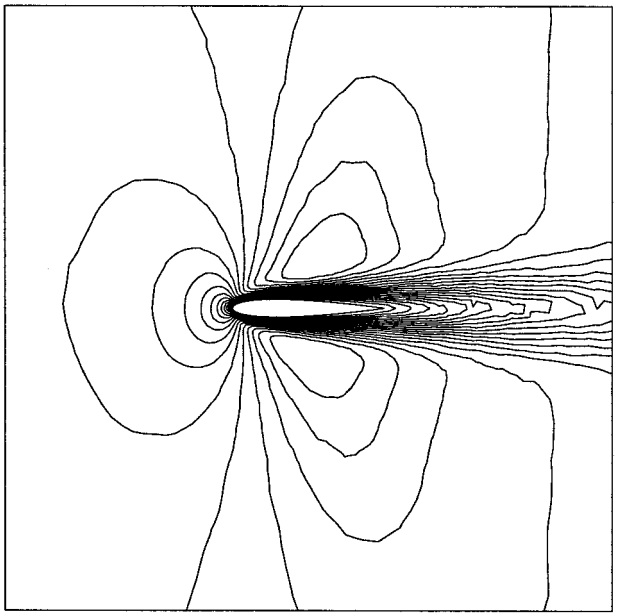

Figure 23. Footbridge scheme: mach isolines around the NACA0012 airfoil ($Re = 500$, $M = 0.85$, $\alpha = 0°$).

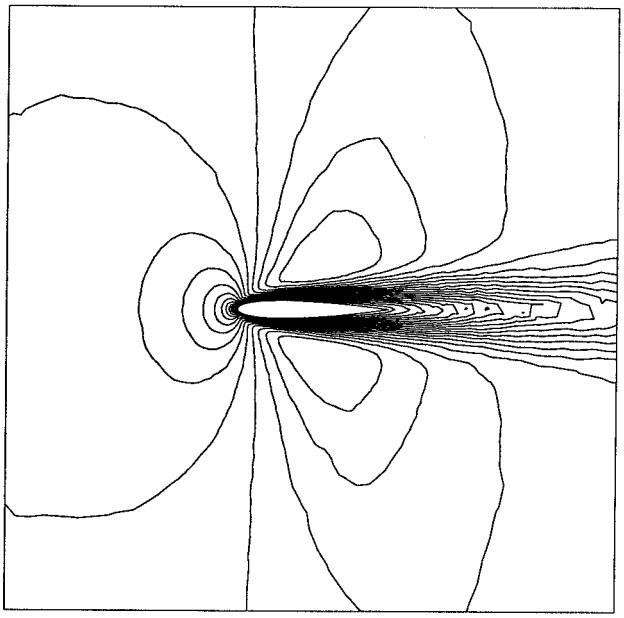

Figure 24. Green–Gauss reconstruction: mach isolines around the NACA0012 airfoil ($Re = 500$, $M = 0.85$, $\alpha = 0°$).

For a time-dependent problem, we need initial conditions that are computed from these values and our aim is to obtain a steady state solution. For this external flow, infinity has been replaced by a large curve and on the inflow boundary condition, ρ_∞ and $(u_\infty, 0)$ are prescribed while on the outflow, Neuman boundary conditions are imposed. On the airfoil, we use a no-slip boundary condition. Let us mention that for the inviscid step, a well boundary condition like $\omega \cdot \vec{v} = 0$ on the airfoil replaces the no-slip condition. We still apply the direct and inverse footbridge to the two components of the velocity although the footbridge we implement does not conserve the boundary conditions since in the finite volume method used for the inviscid step, boundary conditions are imposed by means of the flux through the boundary interface.

Figure 22 shows an enlargement of an unstructured triangulation obtained by the mesh software 'EMC2' developed by Hecht and Saltel [38] and used near the profile to solve the problem. Figure 23 shows a zoom around the section of the computed isomach lines associated with the steady solution reached for a relative error less than 10^{-5}; the time step is fixed such that the CFL number (21) is equal to 0.8. The complex features of the flow are in good agreement with those (figure 6(b)) obtained by Rostand and Stoufflet [14] with a second-order accurate version of the mixed element–volume formulation referred to in the Introduction. An additional aim of this experiment is to examine how well the scheme enforces boundary conditions. One can notice that the proposed scheme correctly recovers the physical viscous layer as does a Green–Gauss reconstruction of the gradient (formulation (4.77) in Barth [39]): in Figure 24, mach number contours computed with this reconstruction on the same mesh are

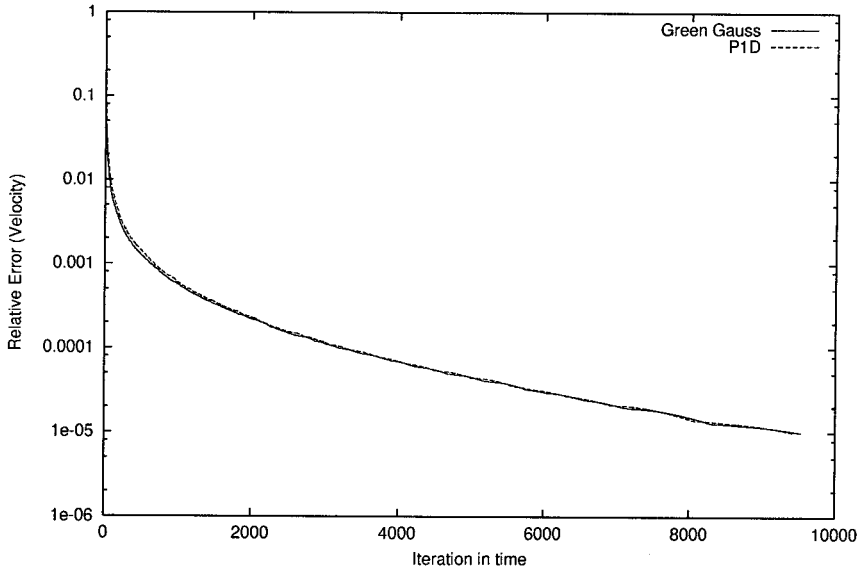

Figure 25. Convergence history for NACA0012 airfoil ($Re = 500$, $M = 0.85$, $\alpha = 0°$).

plotted. The coincidence of both results is very satisfactory. The history of convergence presented in Figure 25 shows the logarithm of the velocity residual

$$\max\left(\frac{|u^{n+1}-u^n|}{|u_\infty|},\frac{|v^{n+1}-v^n|}{|v_\infty|}\right)$$

versus the number of time step and proves that behavior of both schemes is similar.

7. CONCLUDING COMMENTS

In this paper, a multidimensional numerical solver is presented for computing viscous, compressible flows in the context of cell-centered finite volume methods. The principle to discretize the viscous terms stems from associating a finite volume and a finite element representation of the solution on the same mesh called 'footbridge' and from using an operator splitting to separate the convective part from the diffusive part. The convective part is solved with a cell-centered finite volume method and the diffusive part is solved with a finite element scheme.

Numerical experiments show that the resulting algorithm works well and that it is accurate the stable under different conditions without any constraint on the aspect ratios of the volumes in the mesh.

The explorations of the technique developed here are still in progress. Some analytical proofs of the convergence of the footbridge have to be defined and will be presented in a forthcoming paper with results of codes using continuous finite elements but also totally discontinuous elements.

A three-dimensional generalization, which keeps the diagonal property of the mass matrix in formula (2), has been proposed in Ghidaglia and Pascal [40] and has been successfully introduced in an industrial code at EDF by Boucker [41].

ACKNOWLEDGMENTS

This work was performed in the framework of a collaboration between the Département Transferts Thermiques et Aérodynamique of the Division Recherche & Développement (Electricité de France) and the Centre de Mathématiques et de Leurs Applications (ENS Cachan and CNRS). The authors thank the referees for their remarks on the first version of the manuscript.

REFERENCES

1. Van-Leer B. A second order sequel to Godunov's method. *Journal of Computational Physics* 1979; **32**(1): 101–136.
2. Barth T, Frederickson P. Higher order solution of the euler equations on unstructured grids using quadratic reconstruction. In *AIAA-90-0013, 28th Aerospace Science Meeting*, Reno, Nevada, 1990.
3. Abgrall R. An essentially non-oscillatory reconstruction procedure on finite-element type meshes: application to compressible flows. *Computer Methods in Applied Mechanics and Engineering* 1994; **116**(1–4): 95–101. ICOSA-HOM'92 (Montpellier, 1992).
4. Abgrall R. On essentially non-oscillatory schemes on unstructured meshes: analysis and implementation. *Journal of Computational Physics* 1994; **114**(1): 45–58.

5. Godlewski E, Raviart P. *Numerical Approximation of Hyperbolic Systems of Conservation Laws*. Springer: New York, 1996.
6. Eymard R, Gallouët T, Herbin R. *Finite Volume Methods*. Handbook of Numerical Analysis, vol. 7. North-Holland: Amsterdam, 2000; 713–1020.
7. Vignal MH. Convergence of a finite volume scheme for an elliptic–hyperbolic system. *RAIRO Modélisation Mathématique et Analyse Numérique* 1996; **30**(7): 841–872.
8. Herbin R. An error estimate for a finite volume scheme for a diffusion–convection problem on a triangular mesh. *Numerical Methods for Partial Differential Equations* 1995; **11**(2): 165–173.
9. Brooks A, Hughes T. Streamline upwind Petrov–Galerkin formulations for convection dominated flows with particular emphasis on the incompressible Navier–Stokes equations. *Computational Methods in Applied Mechanics and Engineering* 1982; **32**: 199–259.
10. Liu C, McCormick S. The finite volume element method for planar cavity flow. In *Proceedings of the 11th International Conference on CFD*, Williamsburg, *Lecture Notes in Physics*, 323, Dwoyer D, Hussaini M, Voigt R (eds). Springer-Verlag: New York, 1988; 374–378.
11. Cai ZQ, Mandel J, McCormick S. The finite volume element method for diffusion equations on general triangulations. *SIAM Journal of Numerical Analysis* 1991; **28**(2): 392–402.
12. Dervieux A. Steady Euler simulations using unstructured meshes. In *Partial Differential Equations of Hyperbolic Type and Applications*, Geymonat G (ed.). John Wiley: New York, 1987; 33–111.
13. Selmin V. The node-centered finite volume approach: Bridge between finite differences and finite elements. *Computer Methods in Applied Mechanics and Engineering* 1993; **102**(1): 107–138.
14. Rostand P, Stoufflet B. TVD schemes to compute compressible viscous flows on unstructured meshes. In *Nonlinear Hyperbolic Equations—Theory, Computation Methods, and Applications*, Ballmann J, Jeltsch R (eds). Vieweg: Braunschweig, 1989; 510–520.
15. Arminjon P, Madrane A. A mixed finite volume/finite element method for 2-dimensional compressible Navier–Stokes equations on unstructured grids. In *Hyperbolic Problems: Theory, Numerics, Applications. Proceedings of the 7th International Conference*, Zurich, *International Series of Numerical Mathematics*, 129, Fey M, Jeltsch R (eds). Birkhauser Verlag, 1998; 11–20.
16. Carré G, Dervieux A. On the application of FMG to variational approximation of flow problems. *International Journal of Computational Fluid Dynamics* 1999; **12**(2): 99–117.
17. Debiez C, Dervieux A, Mer K, Nkonga B. Computation of unsteady flows with mixed finite volume/finite element upwind methods. *International Journal for Numerical Methods in Fluids* 1998; **27**(1–4): 193–206.
18. Dervieux A, Desideri J-A. Compressible flow solvers using unstructured grids. Technical Report RR-1732, Rapport Institut National de Recherche en Informatique et en Automatique (INRIA), 1992.
19. Farhat C, Lanteri S. Simulation of compressible viscous flows on a variety of mpps: computational algorithms for unstructured dynamic meshes and performance results. *Computational Methods in Applied Mechanics and Engineering* 1994; **119**(1–2): 35–60.
20. Guillard H. *Mixed Element Volume Methods in Computational Fluid Dynamics*. Von Karman Institute, Lecture Series, Bruxelles, 1995.
21. Guillard H, Viozat C. On the behaviour of upwind schemes in the low mach number limit. *Computers and Fluids* 1999; **28**(1): 63–86.
22. Lanteri S. Parallel solutions of compressible flows using overlapping and non-overlapping mesh partitioning strategies. *Parallel Computing* 1996; **22**(7): 943–968.
23. Le Ribault C, Buffat M, Jeandel D. Introduction of turbulent model in a mixed finite volume/finite element method. *International Journal for Numerical Methods in Fluids* 1995; **21**(8): 667–681.
24. Mer K. Variational analysis of a mixed finite/finite volume scheme on general triangulation. Rapport Institut National de Recherche en Informatique et en Automatique (INRIA) 2213, 1994.
25. Idelsohn S, Onate E. Finite volumes and finite elements: Two 'good friends'. *International Journal for Numerical Methods in Engineering* 1994; **37**(19): 3323–3341.
26. Feistauer M, Felcman J, Lukacova-Medvidóva M. Combined finite element-finite volume solution of compressible flow. *Journal of Computers and Applied Mathematics* 1995; **63**: 179–199.
27. Feistauer M, Slavik J, Stupka P. On the convergence of a combined finite volume-finite element method for nonlinear convection–diffusion problems. Explicit schemes. *Numerical Methods for Partial Differential Equations* 1999; **15**(2): 215–235.
28. Feistauer M, Felcman J, Lukacova-Medvidóva M. On the convergence of a combined finite volume-finite element method for nonlinear convection–diffusion problems. *Numerical Methods for Partial Differential Equations* 1997; **13**: 163–190.
29. Feistauer M, Felcman J, Lukacova-Medvidóva M, Warnecke G. Error estimates for a combined finite volume-finite element method for nonlinear convection–diffusion problems. *SIAM Journal of Numerical Analysis* 1999; **36**(5): 1528–1548.

30. Dolejsi V, Angot P. Finite volume methods on unstructured meshes for compressible flows. In *Finite Volumes for Complex Applications*, Benkhaldoum F, Vilsmeier R (eds). Editions Hermes: Roueu, 1996.
31. Feistauer M, Felcman J, Dolejsi V. Numerical simulation of compressible viscous flow through cascades of profiles. *ZAMM Journal of Applied Mathematics and Mechanics* 1996; **76**(Suppl. 4): 297–300.
32. Angot P, Dolejsi V, Feistauer M, Felcman J. Analysis of a combined barycentric finite volume—nonconforming finite element method for nonlinear convection–diffusion problems. *Applied Mathematics*, *Praha* 1998; **43**(4): 263–310.
33. Crouzeix M, Raviart P-A. Conforming and non conforming finite element methods for solving the stationary stokes equations. *RAIRO Analyse Numérique* 1973; **R-3**: 33–76.
34. Ghidaglia J-M, Kumbaro A, Le Coq G, Tajchman M. A finite volume implicit method based on characteristic flux for solving hyperbolic systems of conservation laws. In *Proceedings of the Conference on: Nonlinear Evolution Equations and Infinite-Dimensional Dynamical Systems*, Shangaï, Ta-Tsien L (ed.). World Scientific Publishing Co.: NJ, 1995; 50–65.
35. George A, Liu JW. The evolution of the minimum degree ordering algorithm. *SIAM Review* 1989; **31**(1): 1–19.
36. Ghidaglia J-M, Kumbaro A, Le Coq G. Une méthode volumes finis à flux caractéristiques pour la résolution numérique de lois de conservation. *Comptes Rendus de l'Académie des Sciences Paris Série I* 1996; **332**: 981–988.
37. Glowinski R, Periaux JF. Numerical methods for nonlinear problem in fluid dynamics. In *Supercomputing. State-of-the-Art*, Lichnewski A, Saguez C (eds). North-Holland: Amsterdam, 1987; 381–479.
38. Hecht F, Saltel E. Un Editeur de Maillage et de Contours en 2 dimensions. Rapport Institut National de Recherche en Informatique et en Automatique (INRIA), 1998.
39. Barth T. Aspects of unstructured grids and finite-volume solvers for the Euler and Navier–Stokes equations. Technical Report, Lecture Series, Von Karman Institute for fluid Dynamics, Bruxelles, 1994.
40. Ghidaglia J-M, Pascal F. Passerelles volumes finis—éléments finis, méthodes et applications. Tech. Rep. HT-33/99/0002A, Rapport EDF, 1999.
41. Boucker M. Modélisation numérique multidimensionnelle d'écoulements diphasiques liquide–gaz en régimes transitoire et permanent: méthodes et applications. PhD thesis, ENS de Cachan, 1998.
42. Cai ZQ, McCormick S. On the accuracy of the finite volume element method for diffusion equations on composite grids. *SIAM Journal of Numerical Analysis* 1990; **27**(3): 636–655.

